HOKKAIDO UNIVERSITY

Title	Electromagnetic and thermal characteristics of supplementary-conductor-based no-insulation REBCO pancake coils with comparison to conventional-based ones
Author(s)	Mato, Takanobu; Noguchi, So
Citation	Cryogenics, 131, 103669 https://doi.org/10.1016/j.cryogenics.2023.103669
Issue Date	2023-04
Doc URL	https://hdl.handle.net/2115/94335
Rights	© <2023>. This manuscript version is made available under the CC-BY-NC-ND 4.0 license http://creativecommons.org/licenses/by-nc-nd/4.0/
Rights(URL)	https://creativecommons.org/licenses/by-nc-nd/4.0/
Type	journal article
File Information	Cryogenics_ForHokudai.pdf

Hokkaido University Collection of Scholarly and Academic Papers : HUSCAP

Electromagnetic and thermal characteristics of *supplementary-conductor-based* no-insulation REBCO pancake coils with comparison to *conventional-based* ones

Takanobu Mato[1] and So Noguchi[1]

[1] Graduate School of Information Science and Technology, Hokkaido University, Sapporo 060-0814, Japan

E-mail: mato@em.ist.hokudai.ac.jp

Received xxxxxx
Accepted for publication xxxxxx
Published xxxxxx

Abstract

A no-insulation (NI) winding technique was originally developed in 2011 to enhance the thermal stability of Rare-Earth Barium Copper Oxide (REBCO) pancake coils. Thereafter, several similar techniques of controlling turn-to-turn contact resistance have been proposed, and they can be categorized as the conventional NI winding technique, named a *conventional-based* NI (CNI) technique in this paper. Recently, a few novel winding techniques different from the CNI winding technique but similar have been proposed: an intra-layer no-insulation technique and a conductive-epoxy-resin-coating technique. These techniques utilize supplementary conductors attached or embedded on REBCO coils as bypassing current paths, which is, in this paper, categorized as *supplementary-conductor-based* no-insulation (SNI) techniques. These *conventional-based* and *supplementary-conductor-based* NI techniques have high a potential for high-field applications. As of today, the applications of these NI techniques are nuclear magnet resonance and magnetic field imaging, and compact nuclear reactors. Those applications require a high performance; however, it is still uncertain which NI technique is suitable for which application since the differences in the characteristics are not clarified well. Therefore, we have systematically investigated the thermal stability of SNI REBCO pancake coils with different circuit parameters in this paper. The thermal stability simulation results of SNI REBCO coils were compared with those of CNI REBCO coils. As a result, the SNI REBCO pancake coils are able to be operated with high thermal stability without deteriorating charging performance as long as the turn-to-turn contact resistances between REBCO tapes and supplementary conductors are low.

Keywords: no-insulation winding technique, REBCO pancake coil, supplementary-conductor-based no-insulation technique, thermal stability

1. Introduction

The no-insulation (NI) winding technique proposed by Hahn, et al. has been attracting attention since its proposal because NI Rare-Earth Barium Copper Oxide (REBCO) pancake coils can be avoided thermal runaway and burning-out [1]-[10]. When

a local hot spot appears on a turn of NI REBCO pancake windings, an enforced current can bypass the local hot spot into the adjacent turns through the turn-to-turn contact surface to suppress heat generation [11], [12].

Recently, the metal-as-insulation (MI) technique [13]-[15] the metal-insulator transition (MIT) method [16], and the partial-insulation (PI) technique [17] have also been proposed as a new concept of NI winding technique. Their basic concept is that additional materials are inserted between turns to improve the coil-charging time delay by increasing the turn-to-turn contact resistance. The current behaviors are basically the same as the first-proposed NI technique. These newly proposed NI techniques can also be modeled by parallel RL circuits, and we call these techniques "*conventional-based*" no-insulation (CNI) winding in this paper.

Furthermore, several different types of NI winding techniques that electrical conductors are additionally attached to as current bypass paths have been proposed. Miyazaki, et al. have proposed an insulated REBCO pancake coil whose top surface is coated with electrically conductive epoxy resin [18]. The conductive-epoxy-resin-coated (CERC) REBCO pancake coils showed significantly high thermal stability [19]. The CERC REBCO coils behaved against a normal state transition as a kind of no-insulation winding technique. The RIKEN has proposed a new NI structure for layer-wound REBCO coils, named intra-layer no-insulation (LNI) coils [20]. In the LNI coils, a bypass current flows into copper plates (supplementary conductors) inserted between layers of layer-wound REBCO coils. These CERC and LNI REBCO coils essentially have a common feature different from the ordinary NI pancake coils: i.e., a bypass current passes through supplementary electrical conductors. They have the identical equivalent electrical circuit structure shown later, and they are called "*supplementary-conductor-based*" no-insulation (SNI) winding.

All the NI techniques have great potential for practical high magnetic field applications. Some researchers started to apply these NI techniques to not only magnetic resonance imaging (MRI) [21]-[24] and nuclear magnetic resonance (NMR) [25]-[27] but also compact nuclear fusion [28]. Typically, NI REBCO magnets with small charging delay and high thermal stability have been desired for high-field applications. For instance, some nuclear fusion devices need higher turn-to-turn contact resistance to suppress induced currents due to pulse fields. It is well known that high contact resistance deteriorates thermal stability. The NI structures and parameters should be carefully designed depending on applications. However, it is still uncertain what kind of NI structures is applicable or appropriate for applications with severe requirements, *i.e.*, high thermal stability, short charging delay, and so on.

In this paper, we systematically investigate the characteristics of these NI techniques, categorizing them into two different types of NI structure based on their electrical equivalent circuits as shown in Table 1: the *conventional-based* and the *supplementary-conductor-based* NI structures. The time constant and thermal stability of CNI and SNI coils are simulated as a function of their parameters to clarify how we develop NI REBCO coils towards high thermal stability and short time constant. The detailed electrical and thermal behaviors are also discussed.

2. Simulation models

2.1. Supplementary-conductor-based NI (SNI) REBCO coils

The simulation model of *supplementary-conductor-based* NI (SNI) REBCO coils is explained below, using a CERC REBCO pancake coil as a representative of SNI REBCO coils. Figure 1 shows the schematic view of the CERC REBCO pancake coil

Table 1. Category of SNI and conventional NI coils

Supplementary-conductor-based	Conductive-epoxy-resin-coated [18] Intra-layer no-insulation [20]
Conventional-based	Metal-as-insulation [13]-[15] Metal-insulator-transition material [16] Partial insulation [17]

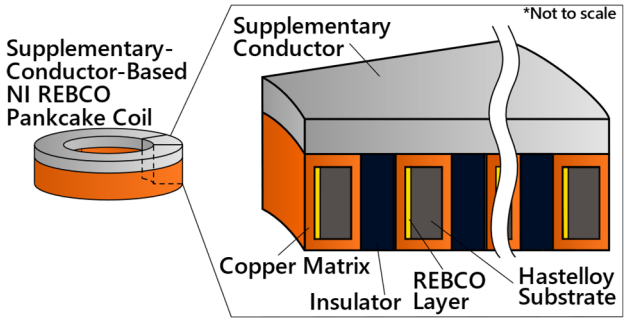


Figure 1. Schematic view of *supplementary-conductor-based* NI (SNI) REBCO pancake coil. A supplementary conductor (conductive epoxy resin [18] in this figure) is attached to the top surface of the insulated REBCO pancake coil as a current bypass path.

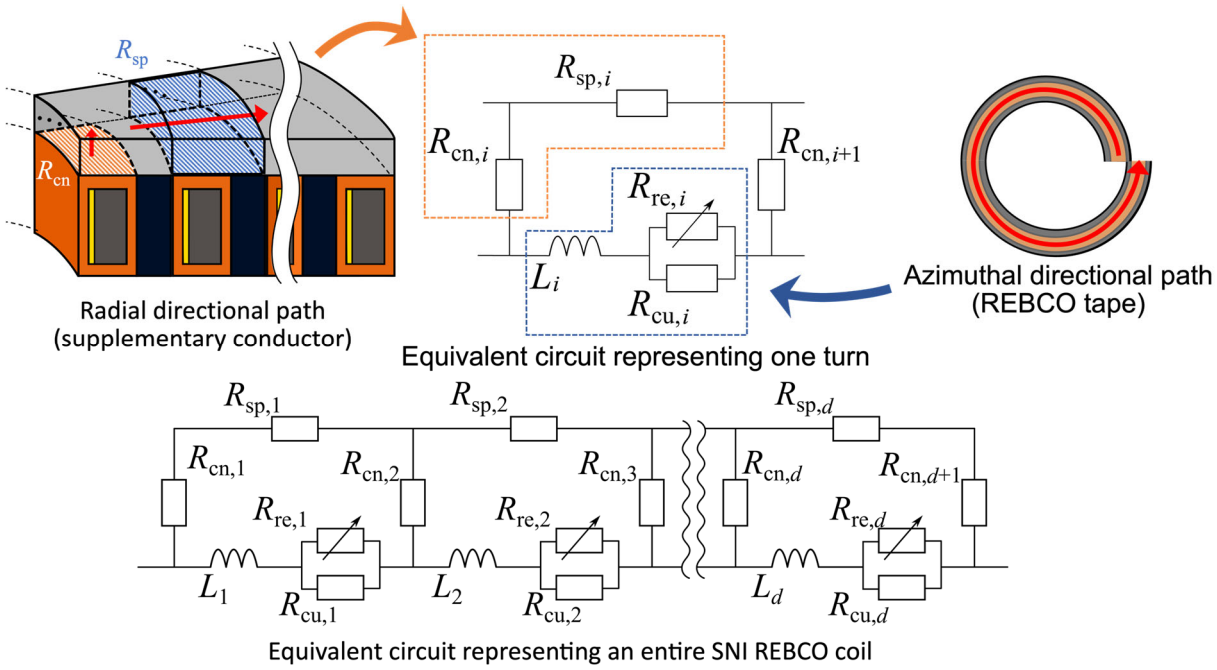


Figure 2. Equivalent circuit of SNI REBCO coil. Each turn is modeled as the combination of fundamental circuit elements. Azimuthal- and radial-directional elements are connected in parallel.

[18]. An insulated pancake coil is wound with REBCO tape, and a conductive epoxy resin is attached onto the surface of the insulated REBCO pancake coil. This structure enables a current to bypass a local hot spot into adjacent turns through the attached supplementary conductor (conductive epoxy resin).

In general, to avoid currents from passing through a local normal zone in SNI REBCO coils, the currents flow into attached supplementary electrical conductors, such as conductive epoxy resins or copper plates, not REBCO tapes. As a major Joule heat generation occurs in the attached supplementary conductors, it is desired that the thermal stability is enhanced, compared with the CNI REBCO pancake coils.

Figure 2 shows an equivalent circuit of CERC (SNI) REBCO coils with current paths through attached supplementary electrical conductors. One circuit element on each winding turn consists of the REBCO layer resistance R_{re}, the copper matrix resistance R_{cu}, and the inductance L [29]. The REBCO layer resistance is calculated from an E-J relationship considering the dependency of temperature and field amplitude and angle, and we used an index power model whose characteristic values were presented in the reference [30]. The attached supplementary conductor resistance and the contact resistance between the supplementary conductor and the REBCO tape are represented as R_{sp} and R_{cn}, respectively. When a local normal zone appears, a bypass current flows into the top-attached conductive epoxy resin through contact surfaces between the pancake coil and the attached epoxy resin. The current paths in the azimuthal and radial directions are represented as a parallel circuit. An equivalent circuit of an entire SNI REBCO coil is shown at the bottom of figure 2.

The attached supplementary conductor resistance R_{sp} of the CERC REBCO coil is given by

$$R_{sp,i} = \rho_{sp} \frac{w}{l_i t_{ep}} \tag{1}$$

where ρ_{sp}, w, l_i, and t_{ep} are the volume resistivity of the attached supplementary conductor (conductive epoxy resin), the thickness of one turn, the REBCO tape length of ith turn, and the thickness of coated conductive epoxy resin, respectively.

The contact resistance R_{cn} is derived from

$$R_{cn,i} = \rho_{cn} \frac{1}{S_{cn,i}} \tag{2}$$

where ρ_{cn} and $S_{cn,i}$ are the REBCO-coil-to-supplementary-conductor contact surface resistivity and the contact surface area of ith turn, respectively.

The presented equivalent circuit structure of the CERC REBCO pancake coil is identical to that of the LNI REBCO coils proposed in [20]. This is the reason why both the CERC and the LNI REBCO coils are categorized into *supplementary-conductor-based* NI REBCO coils.

2.2. Conventional-based NI (CNI) REBCO pancake coils

Figure 3(a) shows the schematic view of a CNI REBCO pancake coil. The REBCO pancake coil is wound without turn-to-turn electrical insulation. An operating current flows into adjacent turns through turn-to-turn contact surfaces when a local normal state transition occurs.

Figure 3(b) shows the equivalent electrical circuit of the CNI REBCO pancake coil, proposed in [31] and used widely. Similarly to the CERC (SNI) REBCO coils, the element equivalent circuit of each winding turn consists of the azimuthal inductance L, the REBCO layer resistance R_{re}, the copper matrix resistance R_{cu}, and the radially directional turn-to-turn contact resistance R_{r}.

The radially directional turn-to-turn contact resistance R_{r} is derived as follows:

$$R_{\mathrm{r},i} = \rho_{\mathrm{r}} \frac{1}{S_{\mathrm{r},i}} \tag{3}$$

where ρ_{r} and $S_{\mathrm{r},i}$ are the radially directional contact resistivity on one turn and the contact surface, respectively.

It is noted that the equivalent circuits of SNI and CNI REBCO coils have the same configuration as each other when $R_{\mathrm{sp}} = R_{\mathrm{r}}$ and $R_{\mathrm{cn}} = 0$.

2.3. Coupling with thermal analysis

To grasp the current behaviors, the circuit equations based on Kirchhoff's laws are solved as an electromagnetic analysis. Furthermore, the thermal analysis is coupled with the electromagnetic analysis to investigate the magnet stability. The thermal conduction equation is solved in the radial direction with a 1-D finite element method. The governing equation is as follows:

$$C \frac{\mathrm{d}T}{\mathrm{d}t} = \lambda \frac{\mathrm{d}^2 T}{\mathrm{d}r^2} + q \tag{4}$$

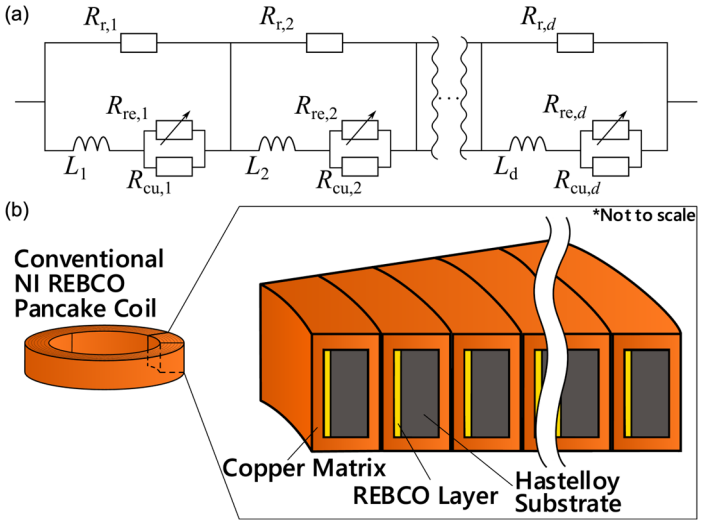


Figure 3. (a) Schematic view and (b) equivalent circuit of ordinary NI REBCO pancake coil.

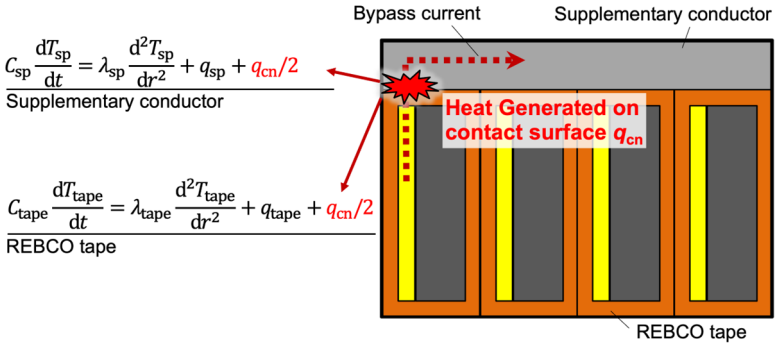


Figure 4. Cross sectional view of CERC REBCO pancake coil. It is assumed that heat generation on contact surface is equally divided to supplementary conductor (conductive epoxy resin) and REBCO winding.

where C, T, λ, and q are the volumetric heat capacity, the temperature, the thermal conductivity, and the heat generation density, respectively. The composite specific heat and thermal conductivity are used for the consideration of multiple materials. Also, the changes in the thermal properties are considered as a function of temperatures [33], [34]. In this paper, it is supposed to be adiabatic as a boundary condition. It is also assumed, as shown in figure 4, that the heat generation on the contact surface between the supplementary conductor and the REBCO winding is equally subdivided into the heat generation q in (4) of both the supplementary conductor and the REBCO winding.

3. Characteristics of SNI REBCO coils

In this section, we have investigated the time constants and thermal stability as a function of the supplementary conductor resistances and the contact resistances. Table 2 lists the specifications of REBCO tape and coil, based on the MRI magnet of [18]. The supplementary conductor resistivity ρ_{sp} changes in the range of 10 nΩ·m to 10 mΩ·m. The contact resistivity ρ_{cn} takes three values: 1.0 μΩ·cm^2, 100 μΩ·cm^2, and 10000 μΩ·cm^2 for the SNI coil. The typical contact resistivity ρ_{cn} of SNI coils is the order of 100-10000 μΩ·cm^2 [20], [32]. The operating conditions are also shown in table 3. It is assumed that the coils are operated at 50 K and cooled by conduction cooling [18]. The operating current is 50 A for the time constant investigation and 300 A for the thermal stability investigation. In the simulation of thermal stability, the whole middle turn (50th turn) transitions into a normal state at t = 0 s. As the coil load factor (I_{op} / I_c) is low, no sequential quench by induced currents occurs [35].

A. Time constants

The time constants are investigated by sudden discharge tests in simulation. The time constants are defined as a time when the magnetic field reaches 36.8 % of initial field after disconnection from the power source. Figure 5 shows the time constants of CERC REBCO pancake coils as a function of the averaged supplementary conductor resistance R_{sp} for three different averaged contact resistance R_{cn} [0.042 μΩ (red), 42 μΩ (green), and 4200 μΩ (blue)]. The time constants of CERC (SNI) coils

Table 2. REBCO tape and coil specifications

Parameters	Units	Values
REBCO tape		
Tape width	[mm]	4.1
Tape thickness	[mm]	0.15
Cu stabilizer thickness (each side)	[μm]	40
REBCO layer thickness	[μm]	2.0
I_c @ 77 K, self field	[A]	130
CERC (SNI) Coil		
Coil i.d.; o.d.	[mm]	500; 536
Number of turns	[turn]	100
Insulator thickness	[μm]	30
Conductive epoxy resin thickness	[mm]	1.0
Conductive epoxy resin resistivity	[Ω·m]	1.0×10^{-8} - 1.0×10^{-2}
Contact resistivity between epoxy resin and REBCO tape	[μΩ·cm^2]	1, 100, 10000
Number of single pancakes	[-]	1
Conventional-based NI (CNI) Pancake Coil		
Coil i.d.; o.d.	[mm]	500; 530
Number of turns	[turn]	100
Radial turn-to-turn contact resistivity	[μΩ·cm^2]	6.3×10^{-4} - 6.3×10^{4}
Number of single pancakes	[-]	1

Table 3. Operating conditions

Parameters	Units	Values
Operating current	[A]	50, 300
Operating temperature	[K]	50
Load factor I_{op}/I_c @300A	[-]	0.60
Normal-state-transitioned turn	[-]	50th

show the non-linear relation against the supplementary conductor resistance for three cases. For instance, in the case of R_{cn} = 4200 μΩ, the time constant does not change in the range of R_{cn} = 1.0 nΩ to 1.0 mΩ because the contact resistance is high enough to dominantly determine the time constants. By increasing the supplementary conductor resistance R_{sp}, the time constants shorten linearly.

The results of *conventional-based* NI coils are also plotted as a black line since the supplementary conductor resistance R_{sp} corresponds to the turn-to-turn contact resistance R_r. Here, it is noted that the radial turn-to-turn contact resistivity ρ_{cn} is changed from 0.63 nΩ·cm^2 to 63 m Ω·cm^2, which enables plotting the result in the same figure. The time constant of CNI REBCO coils decreases linearly with an increase in turn-to-turn contact resistance. In the high turn-to-turn contact resistance region, the time constants are not largely different, compared with the SNI REBCO coils with the same value of the supplementary conductor resistance.

Since the SNI REBCO coils have two parameters, the supplementary conductor resistance R_{sp} and the contact resistance R_{cn}, they potentially have an advantage against the CNI REBCO coils by controlling the parameters to balance the time constant and the thermal stability.

B. Thermal stability

Here, we focus on the temperature rise of the SNI REBCO pancake coils. The coils are operated at 50 K and the operating current of 300 A flows in the coils. When a normal-state zone appears on the 50th turn at t = 0 s, the temperature rises in 2 s are plotted in figure 6 against the supplementary conductor resistance. The temperature rises of the SNI REBCO coil with the actual resistivity of the reference [32] is depicted as point A. Also, the temperature rises of the CNI REBCO coil with the turn-to-turn contact resistivity of 70 μΩ·cm^2, which was measured in [36], is also indicated.

The temperature rise of the CNI REBCO coil (black line) monotonously increases with the turn-to-turn contact resistance, although the CNI REBCO coil turns to the normal state in the high turn-to-turn contact resistance region beyond 2.3 mΩ. This simulation result well agrees with our previous simulation results [37].

In the case of R_{cn} = 4200 μΩ (blue line), the temperature rises are almost constant in a wide region, but it slightly increases with the increase of supplementary conductor resistance R_{sp}. The SNI REBCO coil turns to the normal state entirely when the supplementary conductor resistance exceeds 2.3 mΩ. It is noted that the temperature rise is higher than that of the CNI coils due to its high contact resistance in the whole region.

When the contact resistance R_{cn} is decreased such as 42 μΩ (green) and 0.042 μΩ (red), the increased temperature decreases. Especially, in the case of R_{cn} = 0.042 μΩ (red line), very low temperature rises can be observed, When the supplementary conductor resistance R_{sp} is 0.2 μΩ or higher, the temperature rise is lower than that of the CNI REBCO pancake coil. The mechanism of more stable operation is discussed in Chapter 5.

It is preferred that an SNI REBCO pancake coil has a contact resistivity as low as possible from the viewpoint of the thermal stability. An LNI REBCO coil could have a low contact resistance due to a wide contact area between REBCO tape and copper plate (supplementary conductor). However, the contact resistivity reported in [20] is 25 mΩ·cm^2, and 0.28-1.3 mΩ·cm^2 for the CERC REBCO coil in [32]. These values of the contact resistivity are much higher than the value of 1 μΩ·cm^2, which is at least two orders lower than the actual values. Consequently, it is necessary to develop a new technique for decreasing the contact resistivity or a new structure of SNI REBCO pancake coils.

Furthermore, the electromagnetic characteristics, *i.e.*, the time constants, do not deteriorate in the enclosed region by the dotted orange line in figure 6, compared with the CNI REBCO coils. In that region, the high thermal stability and the short charging delay are well balanced, and such SNI coils possibly have high advantages for applications that need to meet severe requirements.

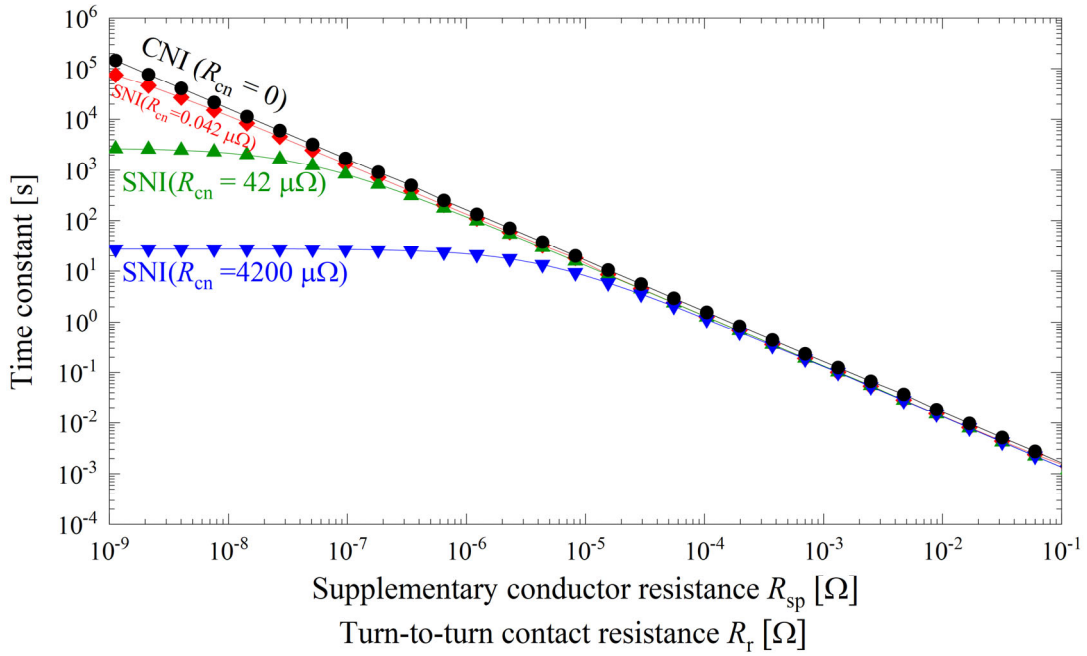


Figure 5. Time constant of *supplementary-conductor-based* NI (SNI) REBCO coils as a function of supplementary conductor resistance R_{sp} for different contact resistances R_{cn}: 0.042 μΩ (red), 42 μΩ (green), and 4200 μΩ (blue). The time constants of *conventional-based* NI (CNI) REBCO coils are also plotted as a function of turn-to-turn contact resistance R_r.

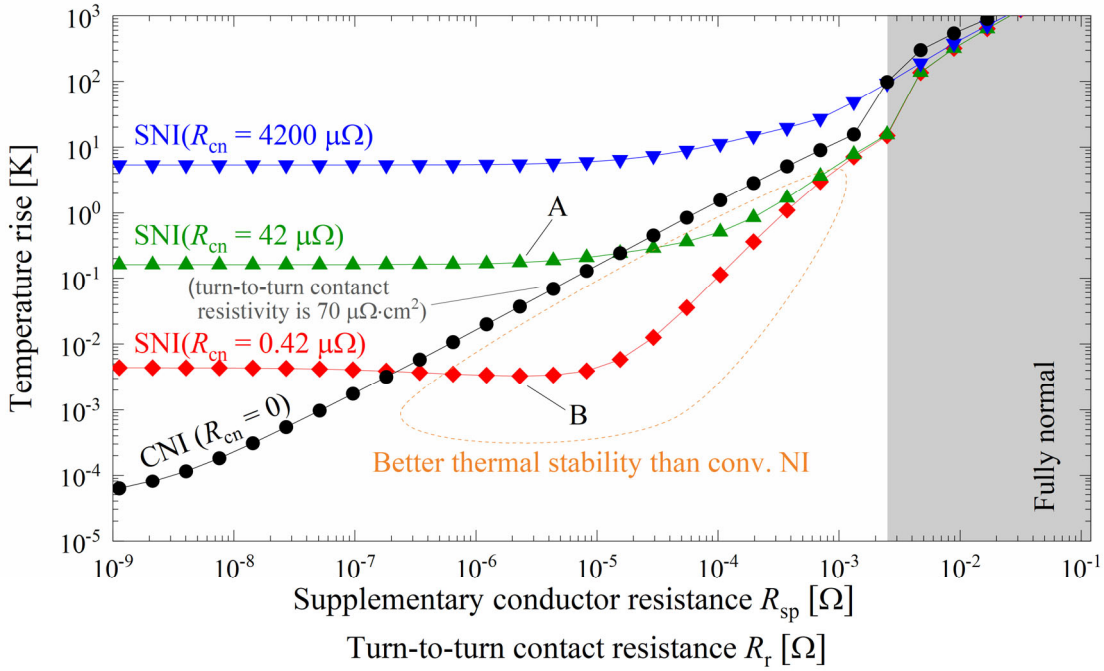


Figure 6. Temperature rises in 2 s after appearance of local normal state transition as function of supplementary conductor resistance R_{sp} for SNI REBCO pancake coils. The black line shows the case of the CNI REBCO pancake coil as a function of turn-to-turn contact resistance R_r. The temperature rises of the CNI REBCO pancake coil with turn-to-turn contact resistivity of 70 μΩ·cm² [36] is indicated as a reference. Blue, green, and red lines show SNI REBCO pancake coils with contact resistances of 4200 μΩ (10000 μΩ·cm²), 42 μΩ (100 μΩ·cm²), and 0.042 μΩ (1.0 μΩ·cm²), respectively. The more stable region of SNI REBCO pancake coils than the CNI REBCO coil is shown with an enclosed dotted orange line. Points A and B are investigated in detail in the next chapter.

4. Current escaping behaviors

The current behaviors are unclear yet, thus, we show the current escaping behaviors and the temperature distributions of CERC REBCO pancake coils to understand the current behaviors for high and low contact resistances (the points A and B in figure 6, respectively). And the improvement of thermal stability is also investigated. Here, it is noted that point A corresponds to SNI REBCO coils with the actual resistivities, and point B is the case with lower contact resistivity.

A. Point A (High contact resistivity)

In case of the point A in figure 6, the contact resistivity ρ_{cn} and the conductive epoxy resin (supplementary conductor) resistivity ρ_{sp} are 100 μΩ·cm^2 and 20 μΩ·m, respectively. The average contact resistance R_{cn} is 42 μΩ, and the average supplementary conductor resistance R_{sp} is 2.3 μΩ. Figure 7 shows the current and thermal transitions on each turn of CERC REBCO pancake coils. The azimuthal current distribution is shown in figure 7(a). At t = 0.1 s, the current is induced around the middle (50th) turn. The current distributes more extensively as time advances. The radially directional bypassing current is shown in figure 7(b). In the beginning, the bypassing current flows into or come out of the conductive epoxy resin (supplementary conductor) within 40 turns. At t = 2 s, the current sharing area widens to 60 turns. The high contact resistivity results in the wide current sharing region.

The Joule heat is generated all over the CERC REBCO pancake coil. Consequently, as shown in figure 7(c), the temperature rise on the 50th is 160 mK in 2 s after the local normal zone appearance.

B. Point B (Low contact resistivity)

In the case of ρ_{cn} = 1.0 μΩ·cm^2 (average R_{cn} = 0.042 μΩ) and ρ_{sp} = 20 μΩ·m (average R_{sp} = 2.3 μΩ), the quench simulation results are depicted in figure 8. After the occurrence of local normal-state transition on the 50th turn, the currents are induced in the adjacent turns, which are slightly larger than that of the high contact resistivity [figure 7(a)]. The induced currents are observed in a smaller area than that of figure 7(a). Figure 8(b) shows the bypassing current distribution. The current bypassing occurs within a small number of turns around the 50th turn. As shown in figure 8(c), the maximum temperature rise is only

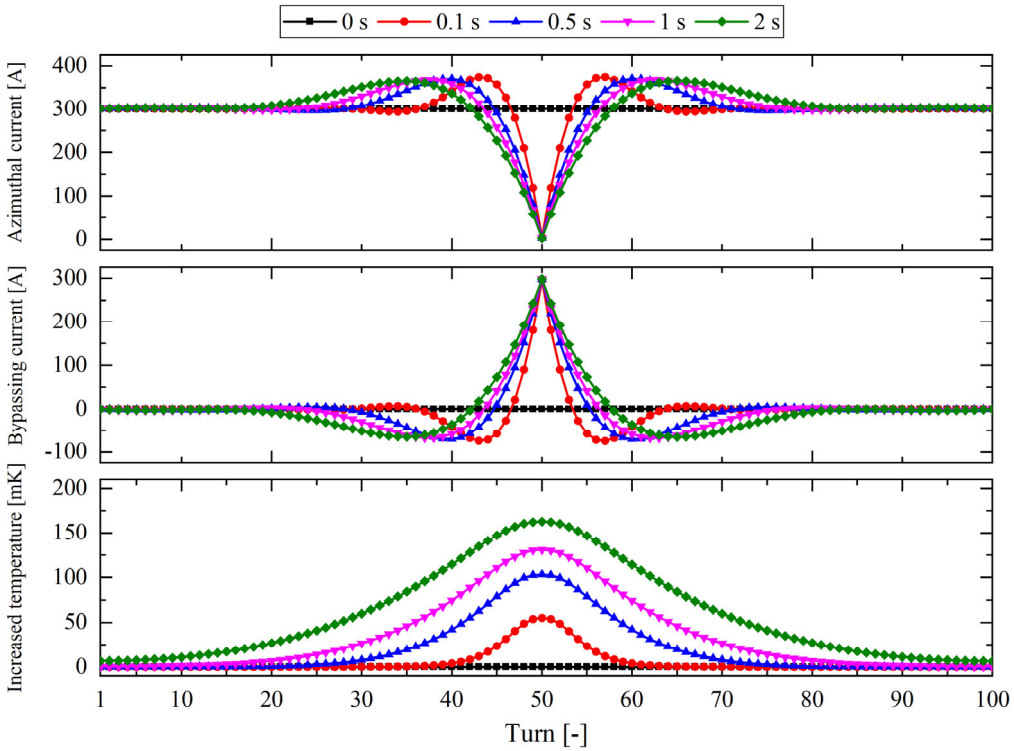


Figure 7. Normal-state transition simulation results when R_{cn} = 42 μΩ and R_{sp} = 2.3 μΩ. (a) Azimuthal current, (b) bypassing current, and (c) temperature time-transitions are depicted on each turn of SNI REBCO pancake coils when a local normal-state transition occurs on 50th turn at t = 0 s.

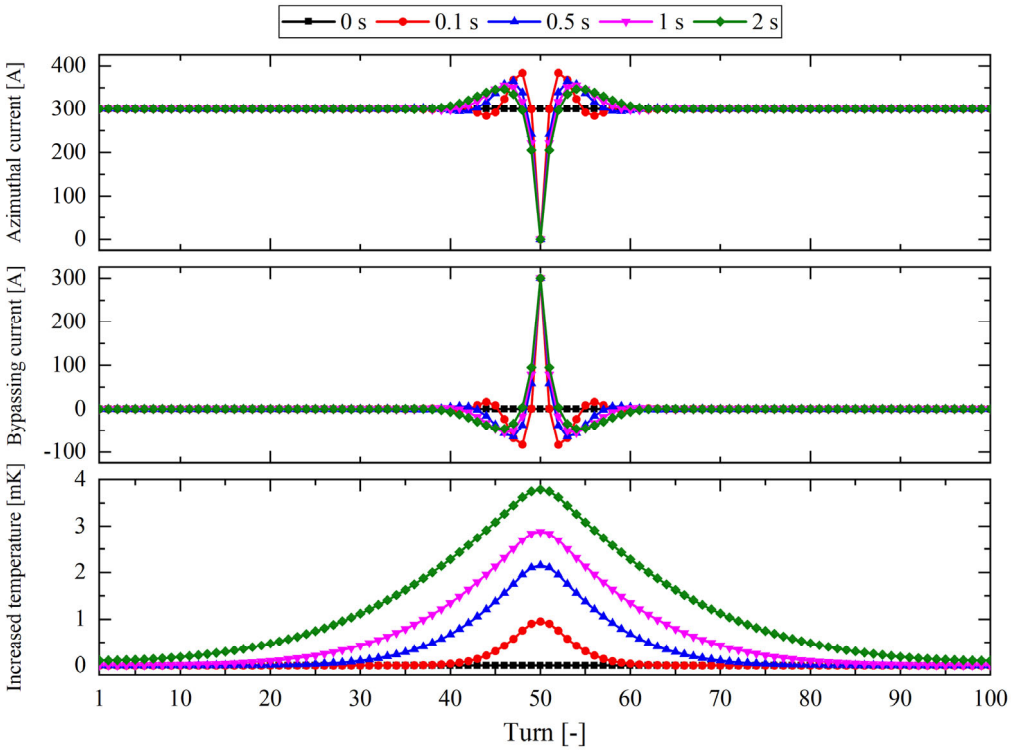


Figure 8. Normal-state transition simulation results when R_{cn} = 0.042 μΩ and R_{sp} = 2.3 μΩ. (a) Azimuthal current, (b) bypassing current, and (c) temperature time-transitions are depicted on each turn of SNI REBCO pancake coils when a local normal-state transition occurs on 50th turn at t = 0 s.

4.7 mK. It is also seen that the temperature distribution is narrower than that of figure 7(c). Due to the low contact resistance and the narrow current-sharing area, the temperature rise is very small.

5. Detailed thermal behavior investigation

In the previous chapter, we showed the current behaviors and the effect of contact resistance on the current distribution of the SNI REBCO coils. Here, the thermal behaviors are further investigated to clarify the mechanism for thermally stable behaviors of the SNI REBCO coils. The results are compared with the CNI REBCO coils as well.

To investigate the thermal characteristics against the supplementary conductor resistance, the ratios of each part to the total heat generation are computed. The definitions of each heat generation ratio are as follows:

$$r_{\mathrm{cn}} = \frac{W_{\mathrm{cn}}}{W_{\mathrm{all}}} \tag{5}$$

$$r_{\mathrm{sp}} = \frac{W_{\mathrm{sp}}}{W_{\mathrm{all}}} \tag{6}$$

$$r_{\mathrm{tape}} = \frac{W_{\mathrm{re}} + W_{\mathrm{cu}}}{W_{\mathrm{all}}} \tag{7}$$

$$r_{\mathrm{r}} = \frac{W_{\mathrm{r}}}{W_{\mathrm{all}}} \tag{8}$$

where W_{cn}, W_{sp}, W_{re}, W_{cu}, W_r, and W_{all} are the Joule heat generation on the contact surface, the supplementary conductor, the REBCO layer, the copper matrix, the turn-to-turn contact surface, and the total heat generation, respectively. Each ratio is plotted as a function of the supplementary conductor resistances for the low and high contact resistances as well as the conventional NI REBCO pancake coil.

A. High contact resistivity

Figure 9 shows the heat generation ratios to the supplementary conductor, the contact surface, and the REBCO tapes, and the temperature rise in the case of the contact resistance R_{cn} = 42 μΩ. In the low supplementary conductor resistance region,

the Joule heat generation on the contact resistance, W_{cn}, is dominant. This means almost all the heat is generated at the contact surface between the REBCO tape and the supplementary conductor. When the supplementary conductor resistance increases, the Joule heat on the supplementary conductor W_{sp} dominates instead of W_{cn}. At the high supplementary conductor resistance region, the Joule heat in the copper takes a relatively large fraction out of total heat. It can be said that the SNI REBCO coils with high supplementary conductor resistance do not work as the self-protection function of the NI winding technique.

It is noted here that the region of the high supplementary-conductor heat generation ratio r_{sp} corresponds to the region where the SNI REBCO coils are thermally more stable than the CNI coils. A large amount of heat is generated in the supplementary conductor, and the generated heat indirectly contributes to the REBCO tape due to the structure of SNI. Therefore, the temperature rise of REBCO tape itself is suppressed, compared to the CNI REBCO pancake coils.

B. Low contact resistivity

Figure 10 shows the heat generation ratios in the case of the contact resistance R_{cn} = 0.042 μΩ. In this case, the contact resistance is much smaller than the previous case. At the low resistance region, r_{cn} is also high. However, the area of high r_{cn} is narrower and the high r_{sp} region is wider than the previous case. Since the contact resistance is low, most of the Joule heat occurs in the supplementary conductor. Therefore, the SNI coils with the low contact resistivity are thermally more stable than CNI REBCO coils in the range of supplementary conductor resistance of 2.3 μΩ or higher in figure 6, which is wider than the case of SNI coils with high contact resistivity.

C. Conventional-based NI coil

Figure 11 illustrates the heat generation ratios against the turn-to-turn contact resistance in the case of the CNI REBCO pancake coils. It is clearly seen that the heat generation on turn-to-turn contact surface W_r dominates in the wide region of turn-to-turn contact resistances R_r from 3 nΩ to 1 mΩ. With the increase of R_r, the Joule heat in copper increases since the current cannot escape through turn-to-turn contact surfaces. The high turn-to-turn contact resistance depresses thermal stability.

6. Conclusion

Several new kinds of no-insulation (NI) winding techniques have been proposed in recent years. From the viewpoint of the equivalent electrical circuit model, these proposed NI winding techniques can be categorized into two groups: the *conventional-based* and the *supplementary-conductor-based* NI REBCO pancake coils. The ordinary NI REBCO coils [1], the MI REBCO coils [13], and the MIT REBCO coils [16] belong to the *conventional-based*. The features of these *conventional-based* techniques were well investigated by experiments and simulations in many papers [38]-[47]. Meanwhile, the conductive-epoxy-resin-coated (CERC) REBCO coil [18], and the intra-layer NI (LNI) REBCO coil [20] are in the group of *supplementary-conductor-based*. The *supplementary-conductor-based* no-insulation (SNI) REBCO coils have supplementary conductors for currents to pass through when a local hot spot appears.

In this paper, we investigated the electromagnetic characteristics and thermal stability of CERC REBCO pancake coils as a representative of SNI REBCO coils. First, the time constant and thermal stability of CERC REBCO pancake coils are systematically investigated as a function of the supplementary conductor resistance, and they are compared with CNI REBCO pancake coils. The simulation results demonstrated that the SNI REBCO coils with a sufficiently small contact resistance were thermally superior to the CNI REBCO coils without deteriorating the charging performance.

The mechanism of the thermal stability was also clarified by showing the Joule heat generation ratios. In case of a low contact resistance, a major heat source is an attached supplementary conductor, because most of the currents easily bypass a local hot spot into it.

Towards practical applications of HTS magnets such as NMR, MRI, and compact nuclear reactors, the SNI REBCO coils have great potential due to their structure, compared to the CNI REBCO pancake coils. The contact resistance (resistivity) between REBCO tapes and supplementary conductors needs to be decreased for such applications, although there is a lot of work to achieve such a low contact resistance. In future work, we need to develop a new technique to lower the contact resistance or to widen the contact surface area to achieve a narrow current-sharing region.

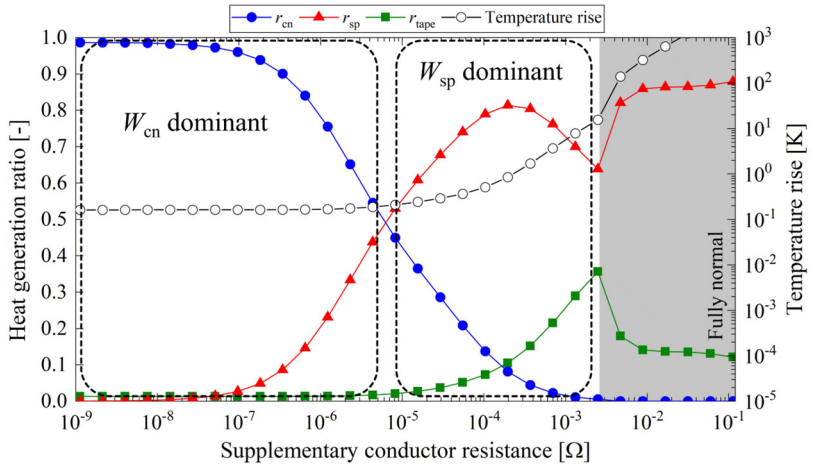


Figure 9. Heat generation ratios of SNI REBCO pancake coil in case of R_{cn} = 42 μΩ.

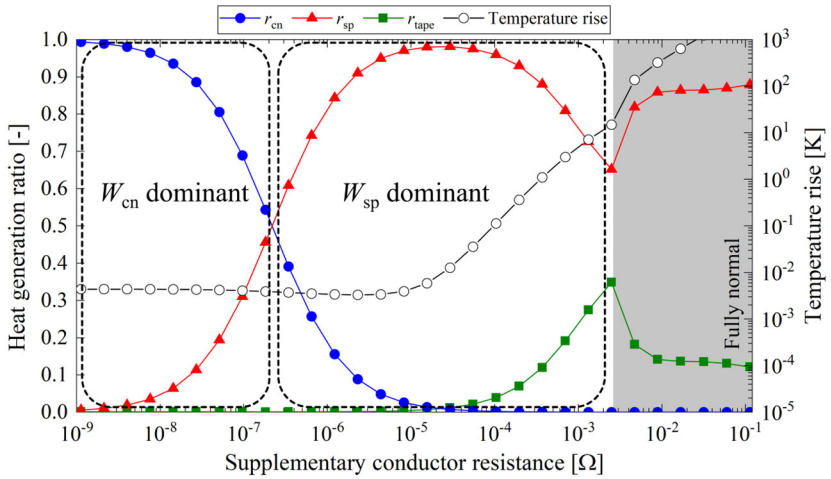


Figure 10. Heat generation ratios of SNI REBCO pancake coil in case of R_{cn} = 0.042 μΩ.

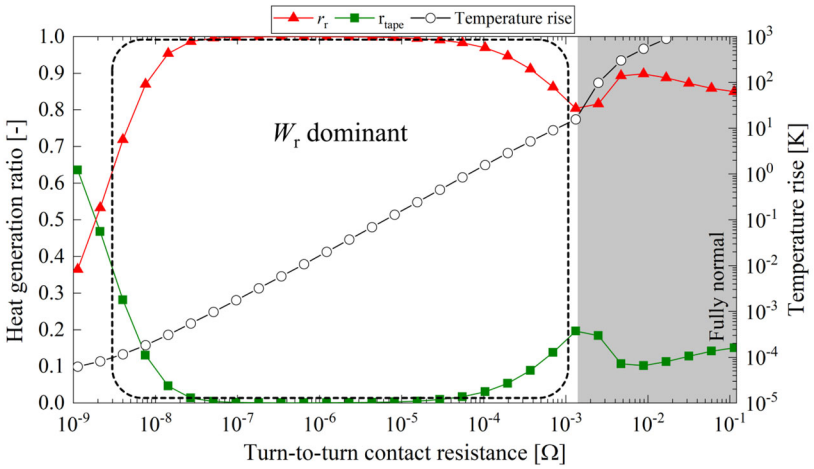


Figure 11. Heat generation ratios of CNI REBCO pancake coil.

Acknowledgment

This work was supported in part by the JSPS KAKENHI under Grant No. 22J20306.

References

[1] Hahn S, Park D K, Bascunan J and Iwasa Y 2011 HTS Pancake Coils Without Turn-to-Turn Insulation *IEEE Trans. Appl. Supercond*. **21** 1592-5
[2] Hahn S, Kim K, Kim K, Hu X, Painter T, Dixon I, Kim S, Bhattarai K R, Noguchi S, Jaroszynski J and Larbalestier D C 2019 45.5-tesla direct-current magnetic field generated with a high-temperature superconducting magnet *Nature* **570** 496–9
[3] Bhattarai K R, Kim K, Kim K, Radcliff K, Hu X, Im C, Painter T, Dixon I, Larbalestier D, Lee S and Hahn S 2020 Understanding quench in no-insulation (NI) REBCO magnets through experiments and simulations *Supercond. Sci. Technol.* **33** 035002
[4] Kim K, Bhattarai K R, Jang J Y, Hwang Y J, Kim K, Yoon S, Lee S and Hahn S 2017 Design and performance estimation of a 35 T 40 mm no-insulation all-REBCO user magnet *Supercond. Sci. Technol*. **30** 065008
[5] Hahn S, Kim Y, Song J, Voccio J, Ling J, Bascuñán J and Iwasa Y 2014 A 78-mm/7-T Multi-Width No-Insulation ReBCO Magnet: Key Concept and Magnet Design *IEEE Trans. Appl. Supercond.* **24** 4602705
[6] Michael P C, Park D, Choi Y H, Lee J, Li Y, Bascuñán J, Noguchi S, Hahn S and Iwasa Y 2019 Assembly and test of a 3-nested-coil 800-MHz REBCO insert (H800) for the MIT 1.3 GHz LTS/HTS NMR magnet *IEEE Trans. Appl. Supercond*. **29** 4300706
[7] Ma J, Geng J and Coombs T A 2017 Flux pumping for non-insulated and metal-insulated HTS coils *Supercond. Sci. Technol.* **31** 015018
[8] Uglietti D, Wesche R and Bruzzone P 2014 Construction and test of a non-insulated insert coil using coated conductor tape *J. Phys. Conf. Ser*. **507** 032052
[9] Iwasa Y and Hahn S 2013 First-cut design of an all-superconducting 100-T direct current magnet *Appl. Phys. Lett.* **103** 253507
[10] Song J-B, Hahn S, Lécrevisse T, Voccio J, Bascuñán J and Iwasa Y 2015 Over-current quench test and self-protecting behavior of a 7 T/78 mm multi-width no-insulation REBCO magnet at 4.2 K *Supercond. Sci. Technol*. **28** 114001
[11] Oki T, Ikeda A, Wang T, Ishiyama A, Noguchi S, Monma K, Watanabe T and Nagaya S 2016 Evaluation on quench protection for no-insulation REBCO pancake coil *IEEE Trans. Appl. Supercond.* **26** 4702905
[12] Ikeda A, Oki T, Wang T, Ishiyama A, Monma K, Noguchi S, Watanabe T and Nagaya S 2016 Transient behaviors of no-insulation REBCO pancake coil during local normal-state transition *IEEE Trans. Appl. Supercond.* **26** 4600204
[13] Lécrevisse T and Iwasa Y 2016 A (RE)BCO pancake winding with metal-as-insulation *IEEE Trans. Appl. Supercond.* **26** 4700405
[14] Bonura M, Barth C, Joudrier A, Troitino J F, Fête A and Senatore C 2019 Systematic study of the contact resistance between REBCO tapes: pressure dependence in the case of no-insulation, metal co-winding and metal-insulation *IEEE Trans. Appl. Supercond.* **29** 6600305
[15] Sohn M, Sim K, Eom B, Ha H, Kim H and Seong K 2018 Controllability of the contact resistance of 2G HTS Coil with metal insulation *IEEE Trans. Appl. Supercond*. **28** 4602705
[16] Kim H, Hur J, Kim S, Kim S, Ko R, Ha D, Kim H M, Joo J and Jo Y 2017 Improvement in stability and operating characteristics of HTS coil using MIT material *IEEE Trans. Appl. Supercond.* **27** 4601704
[17] Choi Y H, Hahn S, Song J B, Yang D G and Lee H G 2011 Partial insulation of GdBCO single pancake coils for protection-free HTS power applications *Supercond. Sci. Technol.* **24** 125013
[18] Miyazaki H, Iwai S, Uto T, Kusano T, Otani Y, Koyanagi K and Nomura S 2019 Over-current test of REBCO pancake coils impregnated with electrically conductive epoxy resin under conduction-cooled conditions *IEEE Trans. Appl. Supercond.* **29** 4602805
[19] Miyazaki H, Iwai S, Uto T, Kusano T, Ishii H, Ito T and Nomura S 2020 Study on a stacked REBCO coil composed of six single pancakes with electrically conductive epoxy resin *IEEE Trans. Appl. Supercond.* **30** 4704105
[20] Suetomi Y, Takahashi S, Takao T, Maeda H and Yanagisawa Y 2019 A novel winding method for a no-insulation layer-wound REBCO coil to provide a short magnetic field delay and self-protect characteristics *Supercond. Sci. Technol.* **32** 045003
[21] Miyazaki H, Iwai S, Otani Y, Takahashi M, Tosaka T, Tasaki K, Nomura S, Kurusu T, Ueda H, Noguchi S, Ishiyama A, Urayama S and Fukuyama H 2016 Design of a conduction-cooled 9.4 T REBCO magnet for whole-body MRI systems *Supercond. Sci. Technol.* **29** 104001
[22] Yokoyama S, Lee J, Imura T, Matsuda T, Eguchi R, Inoue T, Nagahiro T, Tanabe H, Sato S, Daikoku A, Nakamura T, Shirai Y, Miyagi D and Tsuda M 2017 Research and development of the high stable magnetic field ReBCO coil System Fundamental Technology for MRI *IEEE Trans. Appl. Supercond.* **27** 4400604
[23] Parkinson B 2016 Design considerations and experimental results for MRI systems using HTS magnets *Supercond. Sci. Technol*. **30** 014009
[24] Wang X, Wang W, Lei Y, Gao Y, Huang S, Liu X and Zhou Q 2019 Electromagnetic design of 1.5 T no-insulation REBCO coil system charged by multiflux pumps for dedicated MRI *IEEE Trans. Appl*. Supercond. **29** 4601805
[25] Iwasa Y, Bascuñán J, Hahn S, Voccio J, Kim Y, Lécrevisse T, Song J and Kajikawa K 2015 A high-resolution 1.3-GHz/54-mm LTS/HTS NMR magnet *IEEE Trans. Appl. Supercond.* **25** 4301205
[26] Awaji S, Watanabe K, Oguro H, Miyazaki H, Hanai S, Tosaka T and Ioka S 2017 First performance test of a 25 T cryogen-free superconducting magnet *Supercond. Sci. Technol.* **30** 065001
[27] Walsh R M, Slade R, Pooke D and Hoffmann C 2014 Characterization of current stability in an HTS NMR system energized by an HTS flux pump *IEEE Trans. Appl. Supercond.* **24** 4600805
[28] Creely A J, Greenwald M J, Ballinger S B, Brunner D, Canik J, Doody J, Fülöp T, Garnier D T, Granetz R, Gray T K, Holland C, Howard N T, Hughes J W, Irby J H, Izzo V A, Kramer G J, Kuang A Q, LaBombard B, Lin Y, Lipschultz B, Logan N C, Lore J D,

Marmar E S, Montes K, Mumgaard R T, Paz-Soldan C, Rea C, Reinke M L, Rodriguez-Fernandez P, Särkimäki K, Sciortino F, Scott S D, Snicker A, Snyder P B, Sorbom B N, Sweeney R, Tinguely R A, Tolman E A, Umansky M, Vallhagen O, Varje J, Whyte D G, Wright J C, Wukitch S J and Zhu J 2020 Overview of the SPARC tokamak J. *Plasma Phys.* **86** 865860502

[29] Noguchi S 2019 Electromagnetic, thermal, and mechanical quench simulation of NI REBCO pancake coils for high magnetic field generation *IEEE Trans. Appl. Supercond.* **29** 4602607

[30] Ueda H, Imaichi Y, Wang T, Ishiyama A, Noguchi S, Iwai S, Miyazaki H, Tosaka T, Nomura S, Kurusu T, Urayama S and Fukuyama H 2016 Numerical simulation on magnetic field generated by screening current in 10-T-class REBCO coil *IEEE Trans. Appl. Supercond.* **26** 4701205

[31] Liu D, Yong H and Zhou Y 2017 Analysis of charging and sudden-discharging characteristics of no-insulation REBCO coil using an electromagnetic coupling model *AIP Adv.* **7** 115104

[32] Mato T and Noguchi S 2021 Sudden discharging and overcurrent simulations of REBCO coils coated with conductive epoxy resin *IEEE Trans. Appl. Supercond.* **30** 4600705

[33] Lu J, Choi E S and Zhou H D 2008 Physical properties of Hastelloy ® C-276TM at cryogenic temperatures *J. Appl. Phys.* **103** 064908

[34] Copper Development Assoc. Inc. Cryogenic Properties of Copper, 2023, https://www.copper.org/resources/properties/cryogenic/

[35] Miyao R, Igarashi H, Ishiyama A and Noguchi S 2018 Thermal and electromagnetic simulation of multistacked no-insulation REBCO pancake coils on normal-state transition by PEEC method *IEEE Trans. Appl. Supercond.* **28** 4601405

[36] Wang X, Hahn S, Kim Y, Bascuñán J, Voccio J, Lee H and Iwasa Y 2013 Turn-to-turn contact characteristics for an equivalent circuit model of no-insulation ReBCO pancake coil *Supercond. Sci. Technol.* **26** 035012

[37] Noguchi S, Hahn S, Ishiyama A and Iwasa Y 2019 A simple protection evaluation method for no-insulation REBCO pancake coils during local normal-state transition *Supercond. Sci. Technol.* **32** 045001

[38] Gyuráki R, Schreiner F, Benkel T, Sirois F and Grilli F 2020 Fluorescent thermal imaging of a quench in insulated and non-insulated REBCO-wound pancake coils following a heater pulse at 77 K *Supercond. Sci. Technol.* **33** 035006

[39] Kim S B, Saitou A, Joo J H and Kadota T 2011 The normal-zone propagation properties of the non-insulated HTS coil in cryocooled operation *Phys. C* **471** 1428–31

[40] Cubero A, Núñez-Chico A B, Navarro R, Angurel L A and Martínez E 2020 Electromagnetic behaviour and thermal stability of a conduction-cooled, no-insulated 2G-HTS coil at intermediate temperatures *Cryogenics* **108** 103070

[41] Wang X, Wang T, Nakada E, Ishiyama A, Itoh R and Noguchi S 2015 Charging behavior in no-insulation REBCO pancake coils *IEEE Trans. Appl. Supercond.* **25** 4601805

[42] Markiewicz W D, Jaroszynski J, Abraimov D V, Joyner R E and Khan A 2016 Quench analysis of pancake wound REBCO coils with low resistance between turns *Supercond. Sci. Technol.* **29** 025001

[43] Song H and Wang Y 2016 Simulations of nonuniform behaviors of multiple no-insulation (RE)$Ba_2Cu_3O_{7-x}$ HTS pancake coils during charging and discharging *IEEE Trans. Appl. Supercond.* **26** 470010

[44] Wang T, Noguchi S, Wang X, Arakawa I, Minami K, Monma K, Ishiyama A, Hahn S and Iwasa Y 2015 Analyses of transient behaviors of no-insulation REBCO pancake coils during sudden discharging and overcurrent *IEEE Trans. Appl. Supercond.* **25** 4603409

[45] Ueda H, Fukuda M, Hatanaka K, Michitsuji K, Karino H, Wang T, Wang X, Ishiyama A, Noguchi S, Yanagisawa Y and Maeda H 2014 Measurement and simulation of magnetic field generated by screening currents in HTS coil *IEEE Trans. Appl. Supercond.* **24** 4701505

[46] Liu D, Zhang W, Yong H and Zhou Y 2018 Thermal stability and mechanical behavior in no-insulation high-temperature superconducting pancake coils *Supercond. Sci. Technol.* **31** 085010

[47] Wang Y, Chan W K and Schwartz J 2016 Self-protection mechanisms in no-insulation (RE)$Ba_2Cu_3O_x$ high temperature superconductor pancake coils *Supercond. Sci. Technol.* **29** 045007